J|A|C|S
COMMUNICATIONS

Published on Web 03/18/2006

Translucent Thin Film Fe_2O_3 Photoanodes for Efficient Water Splitting by Sunlight: Nanostructure-Directing Effect of Si-Doping

Ilkay Cesar, Andreas Kay, José A. Gonzalez Martinez, and Michael Grätzel*

Institut des sciences et ingénierie chimiques, Ecole Polytechnique Fédérale de Lausanne, CH-1015 Lausanne, Switzerland

Received January 15, 2006; E-mail: michael.graetzel@epfl.ch

Following Fujishima and Honda's[1] light-induced water-splitting experiment with a TiO_2 semiconductor photoanode in 1972, worldwide research has been focused on the conversion of sunlight into hydrogen as a clean and renewable source of energy. Shifting the activity of the photoanode into the visible has been a major challenge so far. Iron oxide (α-Fe_2O_3, or hematite) has unique properties for application in photoelectrolysis reactors. Apart from its ability to absorb a large part of the solar spectrum, its chemical stability, nontoxicity, abundance, and low cost can make it a tempting research target. However, challenges are set by its notoriously short hole diffusion length[2] and the low absorption coefficient due to its indirect band gap (ca. 2.1 eV). In addition, the conduction band of hematite is positioned too positively to reduce water to hydrogen directly. This is overcome by applying an external bias voltage supplied by a dye-sensitized solar cell (dsc) in a tandem-cell configuration.[3−5] The dye cell provides the required potential for hydrogen evolution by absorbing the red part of the solar spectrum which is transmitted by the hematite electrode. Pure hematite is an inefficient photoelectrode, and it has been widely reported that dopants, rendering it either n-type[6−8] or p-type,[9,10] increase the light-to-hydrogen conversion efficiency significantly. In this communication, we report the influence of silicon doping on the water photooxidation efficiency of hematite electrodes prepared by two different methods. Both methods yield translucent thin films composed of Fe_2O_3 nanoleaflets with highly improved photoresponse under illumination with global AM 1.5 solar light. We find that the morphology as well as the photoresponse of the films is significantly influenced by silicon doping.

The iron oxide photoanodes were prepared by ultrasonic spray pyrolysis[4] (USP) and atmospheric pressure chemical vapor deposition (APCVD) based on thermal decomposition of iron(III)-acetylacetonate and iron pentacarbonyl, respectively. Films are grown on transparent, conducting oxide-coated glass with growth rates of 0.6 nm/min for USP and 12 nm/min for APCVD. Tetraethoxysilane (TEOS) was used as silicon dopant.

In the USP method described earlier,[4] the precursor solution was pumped peristaltically through silicone tubing. We found that this influenced the photoresponse of the films, most apparently at lower flow rates. After reducing it from 1.0 to 0.4 mL/min the photocurrent at 1 sun increased by 50% to 1.17 mA/cm^2 at 1.23 V vs RHE (Figure 1a, ca. 375-nm thick film). Replacing the silicone by Tygon tubing, which does not contain silicon, decreased the photoresponse by a factor of 16, but it increased again when a silicone tube was connected in series with the Tygon tube of the pump. Furthermore, adding 0.2 mM TEOS to the deposition solution improves the photoresponse with Tygon tubing (Figure 1b). The film thickness of this TEOS Si-doped sample was 145 ± 20 nm and had a transmittance at 400 and 550 nm of 3.4% and 46%, respectively. This was 3% and 40% at the same wavelengths for an undoped sample of equal thickness. The photoresponse did not significantly increase for thicker TEOS-doped samples. While testing the influence of the tubing material and dopant, the flow rate was kept constant. An improved homogeneity of the deposited film was achieved due to a lower temperature variation along the substrate. By employing an aluminum heating block instead of a tubular oven, the photocurrent density varied less than 5% over a length of 10 cm.

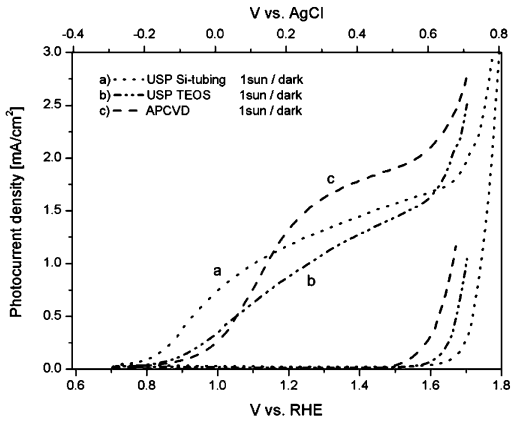

Figure 1. Current−potential curves of Si-doped polycrystalline hematite electrodes on TCO measured vs AgCl: (a) 370-nm thick USP film using silicone tubing; (b) 145-nm thick USP film using Tygon tubing with TEOS as Si-dopant; (c) 170-nm thick APCVD film using TEOS as Si-dopant. Measurement: 1 M NaOH (pH = 13.6)[2]; in darkness and under illumination at 1 sun, AM 1.5 (100 mW/cm^2); scan rate 100 mV/s. The immersed and illuminated anode surface areas were 2.5 and 0.5 cm^2.

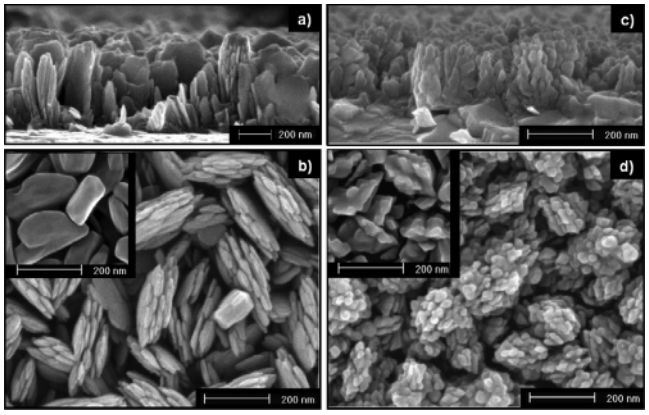

Figure 2. Typical HR-SEM images of Si-doped hematite films on TCO obtained from USP (a,b) and APCVD (c,d): a and c are side-view, b and d top-view images. (b, Inset) Hematite grains for undoped USP (d, Inset) Hematite grains for undoped APCVD electrodes.

Figure 2 (a,b) illustrates the nanostructure obtained from the USP technique with silicone tubing material. This hematite film consists of stacked sheets oriented perpendicularly to the substrate. The

10.1021/ja060292p CCC: $33.50

individual sheets are between 15 and 25 nm thick and, depending on the deposition time used, 50−750 nm long. Changing the tubing material to Tygon increased the crystal size to 200 ± 40 nm in length and 100 ± 15 nm width (inset, Figure 2b). The sheetlike structure was again observed when 0.2 mM TEOS was added to the deposition solution or when silicone tubing was connected in series with Tygon.

These results suggest that the changed morphology and increased photocurrent was caused by an uptake of a silicon compound by the deposition solution from the silicone tubing. This is consistent with improved efficiencies due to a longer residence time at lower flow rates in the tubing. Furthermore, silicone elastomers are known to liberate volatile oligosiloxanes.[12]

The APCVD Si-doped samples give a photocurrent up to 1.45 mA/cm^2 at 1.23 V vs RHE (Figure 1c) and show a dendritic microstructure about 170 nm high with 20−30-nm thick branches (Figure 2 c,d). Pure $Fe(CO)_5$ without silicon dopant gives photocurrents below 1 μA/cm^2 at 1.23 V vs RHE and less developed branches at the electrode surface (inset, Figure 2d).

X-ray diffraction patterns (XRD) of silicon-doped films produced by both techniques have similar hematite signatures superimposed on the tin oxide (casseterite) substrate pattern. In both cases the diffraction peaks of the (110) and to a lesser extent the (300) planes are dominant, indicating a preferred orientation of the (001) basal plane normal to the substrate. This is in accordance with the vertical orientation of the hematite sheets in Figure 2a. A similar preferred orientation has been reported for hematite films consisting of nanowires and nanobelts prepared by thermal oxidation of iron.[13,14] Interestingly, the electrical conductivity is up to 4 orders of magnitude higher along the (001) basal plane than perpendicular to it.[15] The vertical orientation of the well conducting (001) planes in our films may be another reason for the high water-splitting efficiencies obtained.

Different mechanisms for the photoresponse enhancement by the silicon doping can be proposed. Silicon acts as an electron donor due to substitution of Fe^{3+} by Si^{4+} in the hematite lattice and thus improves its electrical conductivity.[6,16,17] At the same time, the increased donor concentration would reduce the width of the space charge layer, generally assumed to be required for charge separation.[18] However, the existence of a space charge layer in our nanocrystalline Fe_2O_3 is questionable due the small particle size.[19] Silicon doping decreases the particle size even further (Figure 2), an effect that has also been described for Si-doped γ-Fe_2O_3,[20] and which can be explained by perturbation of the hematite lattice growth due to the smaller ionic radius of Si^{4+} compared to Fe^{3+}. The presence of silicon reduces the grain size to a level that is commensurate with the hole diffusion length of only a few nanometers in hematite.[2] This renders hole capture by a surface site competitive with recombination, even without the electrical field of a space charge layer. In addition, the smaller grain size increases the specific surface area of the photoanode. Assuming that the overall oxygen evolution is limited by a surface reaction step, this could contribute to higher water oxidation efficiency due to an increased number of active surface sites per unit of substrate area. Leaching of silicon from the Fe_2O_3 surface by the 1 M NaOH electrolyte might activate the surface even at the atomic scale, by creating Fe^{3+} surface sites with additional dangling bonds.[21]

In conclusion, we have improved the photoresponse of nanocrystalline α-Fe_2O_3 films compared to that of the films reported before[4] due to optimized silicon doping. This improvement, measured at 1 sun, amounts to 50 and 90% for the USP and APCVD samples, respectively. The morphology of the nanostructured α-Fe_2O_3 films was strongly influenced by the silicon doping, decreasing the feature size of the nanocrystallites. In a tandem-cell configuration with two series-connected dye-sensitized solar cells providing a bias voltage of 1.4 V and 4 mA/cm^2 at 0.5 sun,[11] the best performing Fe_2O_3 photoanode would yield a solar-to-chemical conversion efficiency of 2.1% based on the heat of hydrogen combustion (upper value = −280 kJ/mol = 1.45 eV/electron).

Further characterization of the α-Fe_2O_3 films such as the Si content is underway, as well as the investigation of alternative dopants, such as Ge, Sn, Pb, Ti, Zr, and Nb. The interface with the TCO substrate is of equal importance, and we are studying the pretreatment of the TCO surface. For example, by depositing a thin interfacial layer,[22] it may be possible to optimize the contact properties. Besides water splitting, other applications, such as gas sensing, photochemical water purification, and nonlinear optics might profit from the unique properties of these new nanocrystalline hematite films.

Acknowledgment. We acknowledge V. Sklover for conducting XRD measurements on our films, R. Humphry-Baker for assisting in our solar simulator calibration, G. Deghenghi for designing the photoelectrochemical measurement cell, and the Centre Interdisciplinaire de Microscopie Electronique for assisting in the SEM imaging. Further we express appreciation to A. P. L. M. Goossens and C. M. Eggleston for many fruitful discussions. We thank the Swiss Federal Office of Energy (SFOE) and Hydrogen Solar Ltd. for financial support.

Supporting Information Available: Experimental procedures and enlarged SEM images. This material is available free of charge via the Internet at http://pubs.acs.org.

References

(1) Fujishima, A.; Honda, K. *Nature* **1972**, *238*, 37.
(2) Kennedy, J. H.; Frese, K. W. *J. Electrochem. Soc.* **1978**, *125*, 709−714.
(3) Grätzel, M. *Nature* **2001**, *414*, 338−344.
(4) Duret, A.; Grätzel, M. *J. Phys. Chem. B* **2005**, *109*, 17184−17191.
(5) Augustynski, J.; Calzaferri, G.; Courvoisier, J. C.; Grätzel, M. *Proc. World Hydrogen Energy Conf., 11th* **1996**, *3*, 2379−2387.
(6) Shinar, R.; Kennedy, J. H. *Sol. Energy Mater.* **1982**, *6*, 323−335.
(7) Sartoretti, C. J.; Alexander, B. D.; Solarska, R.; Rutkowska, W. A.; Augustynski, J.; Cerny, R. *J. Phys. Chem. B* **2005**, *109*, 13685−13692.
(8) Sanchez, C.; Sieber, K. D.; Somorjai, G. A. *J. Electroanal. Chem.* **1988**, *252*, 269−290.
(9) Ingler, W. B.; Khan, S. U. M. *Int. J. Hydrogen Energy* **2005**, *30*, 821−827.
(10) Ingler, W. B.; Khan, S. U. M. *Thin Solid Films* **2004**, *461*, 301−308.
(11) Grätzel, M. *Chem. Lett.* **2005**, *34*, 8−13.
(12) Andersson, L. H. U.; Hjertberg, T. *J. Appl. Polym. Sci.* **2003**, *88*, 2073−2081.
(13) Fu, Y. Y.; Wang, R. M.; Xu, J.; Chen, J.; Yan, Y.; Narlikar, A. V.; Zhang, H. *Chem. Phys. Lett.* **2003**, *379*, 373−379.
(14) Wen, X.; Wang, S.; Ding, Y.; Wang, Z. L.; Yang, S. *J. Phys. Chem. B* **2005**, *109*, 215−220.
(15) Iordanova, N.; Dupuis, M.; Rosso, K. M. *J. Chem. Phys.* **2005**, *122*.
(16) Kennedy, J. H.; Shinar, R.; Ziegler, J. P. *J. Electrochem. Soc.* **1980**, *127*, 2307−2309.
(17) Sanchez, H. L.; Steinfink, H.; White, H. S. *J. Solid State Chem.* **1982**, *41*, 90−96.
(18) Itoh, K.; Bockris, J. O. *J. Electrochem. Soc.* **1984**, *131*, 1266−1271.
(19) Cahen, D.; Hodes, G.; Grätzel, M.; Guillemoles, J. F.; Riess, I. *J. Phys. Chem. B* **2000**, *104*, 2053−2059.
(20) Zhu, Y. H.; C., Li, Z. *Mater. Chem. Phys.* **1997**, *51*, 169.
(21) Nakamura, R.; Okamura, T.; Ohashi, N.; Imanishi, A.; Nakato, Y. *J. Am. Chem. Soc.* **2005**, *127*, 12975−12983.
(22) Kay, A.; Grätzel, M. *Chem. Mater.* **2002**, *14*, 2930−2935.

JA060292P